International Journal of Mass Spectrometry 297 (2010) 46–54

Contents lists available at ScienceDirect

International Journal of Mass Spectrometry

journal homepage: www.elsevier.com/locate/ijms

Infrared spectra and density functional theory calculations for $Mn^+–(CH_4)_n$ ($n = 1–6$) clusters

Viktoras Dryza*, Evan J. Bieske*

School of Chemistry, The University of Melbourne, Victoria 3010, Australia

ARTICLE INFO

Article history:
Received 1 April 2010
Received in revised form 11 May 2010
Accepted 12 May 2010
Available online 21 May 2010

Keywords:
Transition metal cation
Methane
Cluster
Infrared spectroscopy

ABSTRACT

Infrared spectra are measured for the mass-selected $Mn(CH_4)_n^+$ ($n = 1–6$) clusters in the C–H stretch region (2700–3100 cm^{-1}) by monitoring photofragment ions. Accompanying density functional theory calculations are performed for possible structural isomers, including the $Mn^+–(CH_4)_n$ ion-molecule complexes in which the ligands are attached to the Mn^+ ion in an η^3 configuration, and the inserted $H–Mn–CH_3^+–(CH_4)_{n-1}$ complexes. The experimental infrared spectra for all species are dominated by a single band, appearing at 2836 cm^{-1} for $n = 1$ and progressively shifting to 2880 cm^{-1} for $n = 6$. The observed infrared spectra match predicted spectra for $Mn^+–(CH_4)_n$ ion-molecule complexes containing Mn^+ in its ^7S ($4s^1 3d^5$) electronic ground state, with the dominant band corresponding to the totally symmetric C–H stretching vibrations of the attached CH_4 ligands. No evidence was found for clusters containing the Mn^+ cation in its ^5S ($4s^1 3d^5$) electronic state. In larger clusters, the CH_4 ligands are generally bound to the Mn^+ ion such that adjacent $Mn^+\cdots C$ bonds are approximately at right angles to one another taking advantage of partial 4s/4p hybridization to minimise the CH_4 molecules' repulsive interaction with the half-filled 4s orbital of Mn^+.

1. Introduction

The transformation of saturated hydrocarbons, such as methane (CH_4), to form further useful chemicals such as alcohols and ketones is a challenging exercise requiring the activation of a strong C–H σ-bond to make a more reactive and more readily functionalized bond [1,2]. In practice, the process of C–H bond activation is often accomplished using systems containing transition metal atoms. One appealing approach to understanding the fundamental mechanistic details of C–H bond activation by transition metals involves investigating the interaction between CH_4 molecules and a transition metal cation (TM^+) in the gas-phase where the complicating influences of solvent and substrate are eliminated. This can be done either by studying ion-molecule reactions or by forming and characterising ion-neutral complexes. This latter approach is taken for the current spectroscopic investigation of the $Mn^+(CH_4)_n$ clusters. The restricted size and isolated nature of these complexes invites high-level experimental and computational investigations to provide reliable information on the underlying energetics, geometries, and mechanisms.

Different structures and reaction pathways are possible for the $TM(CH_4)_n^+$ species. In the first instance, an ion-molecule complex can be formed (i.e., $TM^+–(CH_4)_n$), whereby intact CH_4 molecule(s) are attached to the TM^+ ion through electrostatic and induction interactions, augmented by cohesion arising from electron donation from the ligands to available orbitals on the TM^+ ion [3]. These orbital interactions play a crucial role in deciding the coordination of the ligands and for a first row TM^+ ion depend on the occupation and configuration of the 4s and 3d orbitals. Not only are these ion-molecule complexes important as entrance channel structures for possible C–H σ-bond activation processes, they are also relevant to methane storage in porous materials containing exposed TM^+ sites [4,5]. In order to understand the operative interactions, binding energies for CH_4 ligands attached to a TM^+ ion (Ti^+, Fe^+, Co^+ and Ni^+) have been measured using either high pressure mass spectrometry or threshold collision induced dissociation, often in conjunction with quantum chemical calculations to help identify the lowest energy structures [6–11]. The coordination of the CH_4 ligands and the electronic configuration of the core TM^+ ions has been elucidated by correlating experimental binding energies with calculated values.

In some instances, C–H σ-bond activated pathways can proceed from an ion-molecule complex including insertion of the TM^+ ion into one or more C–H bonds to form an inserted complex (e.g., $H–TM–CH_3^+–(CH_4)_{n-1}$), or insertion into two or more C–H bonds resulting in dehydrogenation (e.g., $TM–(CH_3)_2^+–(CH_4)_{n-2} + H_2$)

* Corresponding authors.
E-mail addresses: vdryza@unimelb.edu.au (V. Dryza), evanjb@unimelb.edu.au (E.J. Bieske).

1387-3806/$ – see front matter © 2010 Elsevier B.V. All rights reserved.
doi:10.1016/j.ijms.2010.05.017

[12]. One of the fascinating aspects of TM^+ ion chemistry is the availability of low-lying electronic states, meaning that several potential energy surfaces (PESs) associated with different electron spin multiplicity can be involved in determining the final products and their structures [13]. For example, van Koppen et al. [8] have shown that ion-molecule complexes are formed when two CH_4 ligands are attached to Ti^+, yet under certain experimental conditions, addition of the third CH_4 results in sequential insertion into two C–H bonds on separate ligands, followed by dehydrogenation. This cluster assisted σ-bond activation requires a crossing from a quartet to a doublet PES.

Infrared photodissociation (IR-PD) spectroscopy is a powerful way to probe the structural characteristics of metal cation bearing clusters in the gas-phase [14]. So far only a limited number of spectroscopic studies have been performed to complement the binding energy data for complexes consisting of methane molecules attached to a metal cation. In particular, our group and that of Metz have collected IR-PD spectra in the C–H stretch vibrational region (~2600–3100 cm^{-1}) of the $Al(CH_4)_n^+$ (n = 1–6) and $Fe(CH_4)_n^+$ (n = 3–4) complexes, respectively [15,16]. Structural insights can be derived from the spectra as the vibrational frequencies of the CH_4 ligands depend on the strength and characteristics of the intermolecular bond, i.e., attachment to either a TM^+ or H–TM–CH_3^+ core, spin multiplicity, and ligand coordination. Theoretical and IR-PD studies of the $Al(CH_4)_n^+$ (n = 1–6) and $Fe(CH_4)_n^+$ (n = 3–4) complexes concluded that the CH_4 molecules were respectively attached in η^3 and η^2 configurations to the metal cation.

In this paper we describe a combined IR-PD spectroscopy and density functional theory (DFT) study of the $Mn(CH_4)_n^+$ (n = 1–6) complexes. Previously, no experimental data existed for these complexes, although theoretical investigations of the $MnCH_4^+$ species have been undertaken by Michelini et al. [17,18] who examined the PESs for complexes containing Mn^+ in both the ground ^7S ($4s^13d^5$) state and excited ^5S ($4s^13d^5$) state using DFT and *ab initio* methods. On the septet surface an η^3-bound Mn^+–CH_4 complex is predicted to be the minimum energy structure (Fig. 1a), with formation of the inserted H–Mn^+–CH_3 structure (Fig. 1c) being significantly endothermic. On the quintet surface, a Mn^+–CH_4 complex is also the minimum energy structure, but now C–H bond insertion is predicted to be either slightly exothermic (DFT) or endothermic (*ab initio*), relative to the ^5S Mn^{2+} CH_4 asymptote. Both DFT and CCSD(T) methods predict the ^7S Mn^+–CH_4 complex to be the global minimum energy structure.

The current study aims to test the earlier calculations of Michelini et al. for the Mn^+–CH_4 complex [17,18] and to explore the consequences of attaching more CH_4 ligands to the Mn^+ ion in regards to ligand coordination, spin multiplicity changes, and C–H σ-bond insertion. As shown below, the IR-PD spectra of the $Mn(CH_4)^+$ (n = 1–6) clusters match those calculated for ion-molecule complexes containing the Mn^+ ion in its ground ^7S state, consistent with the energetics of the isomers calculated by DFT.

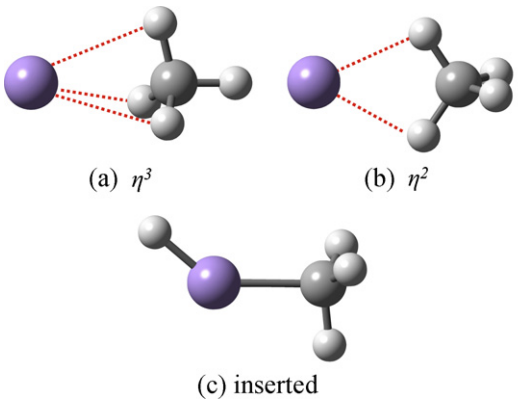

Fig. 1. Bonding motifs for $(MnCH_4)^+$: (a) η^3, (b) η^2 and (c) inserted.

2. Experimental and computational approaches

2.1. Experimental approach

The IR-PD spectra of the $Mn(CH_4)_n^+$ (n = 1–6) complexes were recorded by scanning an IR laser over the C–H stretch region (2700–3100 cm^{-1}) and monitoring production of photofragments in a tandem mass-spectrometer. General details of the IR-PD set-up have been given previously [19]. Briefly, the $Mn(CH_4)_n^+$ complexes were generated in a pulsed supersonic expansion of pure CH_4 gas (8 bar) passed over a laser-ablated manganese rod. Whether our ablation source creates a significant proportion of electronically excited Mn^+ ions is unknown. The desired ions were mass-selected by a quadrupole mass filter and deflected through 90° by a quadrupole bender into an octopole ion guide where they were overlapped by the counter-propagating IR output of a pulsed, tunable OPO (Continuum Mirage 3000, bandwidth of 0.017 cm^{-1}). The resulting $Mn(CH_4)_{n-m}^+$ photofragments were mass-selected by a second quadrupole mass filter and passed through to the ion detector. The IR-PD spectra were recorded using the m = 1 channel for n = 1–3 clusters and the m = 2 channel for the n = 4–6 clusters. Spectra recorded using the m = 1 channel for n = 4–6 displayed identical features to the m = 2 spectra, but had an inferior signal-to-noise ratio.

2.2. Computational approach

Geometry optimization and harmonic vibrational frequency calculations for the $Mn(CH_4)_n^+$ complexes were performed using density functional theory (DFT) and the B3LYP functional within the Gaussian 09 suite of programs [20]. For Mn^+, the 10 electron Stuttgart relativistic pseudopotential was used in conjunction with the Stuttgart/Dresden (SDD) basis set augmented with two f-type and one g-type polarization functions [21,22]. The aug-cc-pVTZ basis set was used for the H and C atoms. Pure spherical harmonic functions were used with these basis sets and the calculations were conducted on a large grid of size (99, 590).

Several structural isomers were considered for each of the $Mn(CH_4)_n^+$ complexes. Ion-molecule complexes comprising intact CH_4 ligands coordinated with the Mn^+ ion were considered for n = 1–6, whereas structures containing an inserted H–Mn–CH_3^+ sub-unit were only considered for the n = 1–3 species. Both η^2 or η^3 bonding configurations were considered for CH_4. As shown in Fig. 1b, for η^2 bonding, the ion sits along the C_2 axis that bisects two C–H bonds, whereas for η^3 bonding the ion is situated along the C_3 axis lying midway between three C–H bonds (Fig. 1a).

Structural isomers for n = 1–6 were calculated with a septet spin multiplicity, while the n = 1–3 complexes were also calculated with a quintet spin multiplicity. A natural population analysis (NPA) was performed for all isomers to help identify the electronic configuration of the Mn^+ ion and charges on the atoms [23]. In all cases the septet and quintet spin multiplicities corresponded to the ^7S ($4s^13d^5$) and ^5S ($4s^13d^5$) electronic states of Mn^+, respectively. For Mn^+, the DFT calculations predicted the ^5S state to lie 87 kJ/mol above the ground ^7S state, underestimating somewhat the experimental value of 113 kJ/mol [24].

Binding energies for the attached CH_4 ligand were computed for all isomers assuming conservation of spin multiplicity during dissociation. In each case the binding energy was corrected for vibrational zero-point energy (ZPE). Simulated infrared spectra in

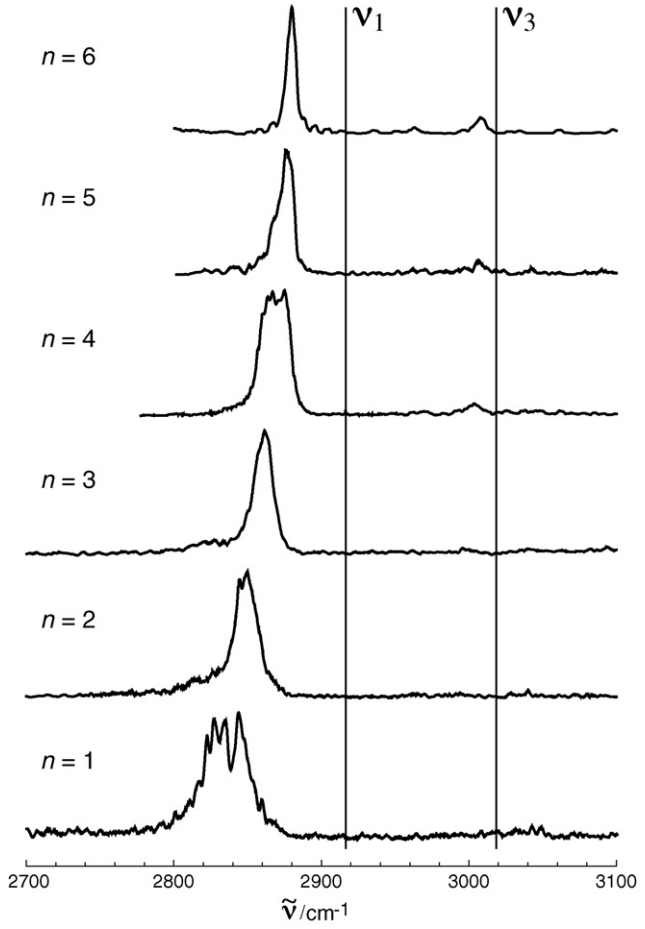

Fig. 2. Infrared photodissociation spectra for the $Mn(CH_4)_n^+$ (n = 1–6) complexes. Frequencies for the $\nu_1(a_1)$ and $\nu_3(t_2)$ bands of the free CH_4 molecule are indicated by the vertical lines.

the C–H stretch region were generated so that comparisons could be made with the experimental spectra. To do this, the calculated harmonic vibrational frequencies were scaled by 0.9625, the factor required to reconcile the calculated frequency of the $\nu_1(a_1)$ totally symmetric C–H stretch vibrational mode in the free CH_4 molecule with the experimental value (2917 cm^{-1} [25]). The simulated vibrational peaks were represented by Gaussian functions with heights proportional to the calculated infrared intensities and a 10 cm^{-1} full-width half-maximum.

Table 1
Experimental wavenumbers (cm^{-1}) for vibrational bands of the $Mn(CH_4)_n^+$ complexes. Each band is labelled as either strong (s) or weak (w) according to its intensity.

n	Band wavenumber (cm^{-1})
1	2836(s)
2	2849(s)
3	2861(s)
4	2870(s), 3003(w)
5	2876(s), 3006(w)
6	2880(s), 3008(w)

3. Results and discussion

3.1. Experimental infrared spectra

The IR-PD spectra of the $Mn(CH_4)_n^+$ (n = 1–6) complexes over the 2700–3100 cm^{-1} range are shown in Fig. 2. Vibrational band positions are summarised in Table 1. In general appearance, the spectra are similar to those of the $Al(CH_4)_n^+$ (n = 1–6) complexes [15]. Each of the spectra is dominated by a single band that shifts progressively to higher frequency with the number of attached CH_4 ligands, commencing at 2836 cm^{-1} for n = 1 and reaching 2880 cm^{-1} for n = 6. As explained below, this dominant band is associated with the symmetric C–H stretch vibrational mode of CH_4 molecules attached to a ^7S Mn^+ core. In the free CH_4 molecule the $\nu_1(a_1)$ mode has a frequency of 2917 cm^{-1} [25] (marked by a vertical line in Fig. 2) and is IR inactive; the mode becomes strongly IR active in the presence of a metal cation due to the reduced symmetry and charge-induced polarization [15]. A second weak band, appearing at ~3005 cm^{-1} for the n = 4–6 complexes, is presumably associated with the $\nu_3(t_2)$ C–H stretching mode, which for free CH_4 occurs at 3019 cm^{-1} [25] (also marked by a vertical line in Fig. 2).

3.2. DFT calculated isomers and predicted infrared spectra

The following sections describe the structural isomers examined by DFT for each of the $Mn(CH_4)_n^+$ species. For convenience, we designate the ion-molecule Mn^+–$(CH_4)_n$ complex and the inserted

Table 2
DFT calculated properties for the $Mn^+(CH_4)_n$ isomers including the electronic state/molecular symmetry, relative energy, CH_4 binding energy, intermolecular $Mn^+\cdots C$ bond distance, and $\nu_1(a_1)$ C–H stretch vibrational frequency.

n	Isomer	Electronic state	ΔE (kJ/mol)	D_0 (kJ/mol)	$Mn^+\cdots C$ distance (Å)	$\nu_1(a_1)$	
						Calculated (cm^{-1})	Experimental (cm^{-1})
1	7-C	$^7A_1$ (C_{3v})	0	34	2.64	2849	2836
	5-C	$^5A_1$ (C_{3v})	+56	66	2.24		
	5-I	$^5A'$ (C_s)	+102	–	–		
	7-I	$^7A_1$ (C_{3v})	+163	–	–		
2	7-C	^7A (C_2)	0	21	2.77	2864	2849
	5-C	$^5A_{1g}$ (D_{3d})	+2	74	2.11		
	5-I	$^5A'$ (C_s)	+69	54	2.42		
	7-I	^7A (C_1)	+159	25	2.66		
3	7-C	^7A (C_3)	0	13	2.87	2873	2861
	5-C	$^5A_1$ (C_{2v})	+12	3	2.30, 2.61		
	5-I	$^5A'$ (C_s)	+69	23	2.55		
	7-I	^7A (C_1)	+155	18	2.73		
4	7-C	^7A (C_2)	–	13	2.95, 3.09	2883	2870
5	7-C	$^7A'$ (C_{3h})	–	5	3.16, 3.10	2889	2876
6	7-C	$7A_1$ (D_3)	–	4	3.21	2893	2880

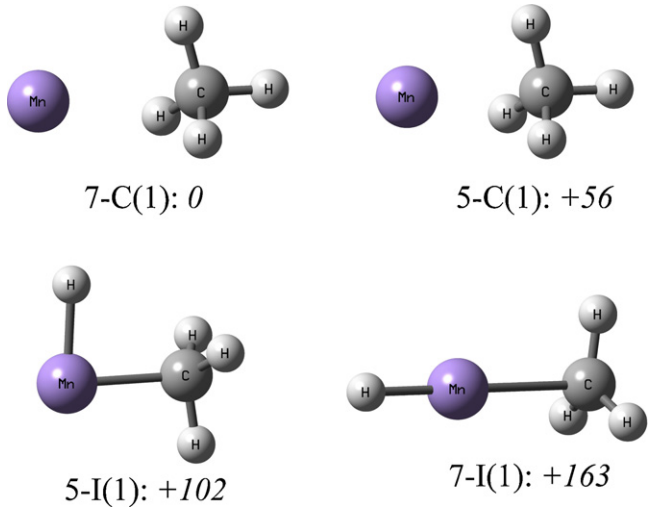

Fig. 3. DFT calculated isomers for $MnCH_4^+$. Relative energies for each structure are given in kJ/mol.

$H–Mn–CH_3^+–(CH_4)_{n-1}$ complex as *M*-C(*n*) and *M*-I(*n*), respectively, where *M* is the spin multiplicity (either 7 or 5), corresponding to complexes containing either a ^7S ($4s^1 3d^5$) or a ^5S ($4s^1 3d^5$) Mn^+ ion.

For both the uninserted and inserted complexes we found only one stable coordination geometry for the CH_4 ligands, although occasionally structural isomers were located quite close in energy (<2 kJ/mol) differing only by internal rotation of the η^3 CH_4 ligands about the $Mn^+\cdots CH_4$ bonding axis. As the barrier for this internal rotation is low and the IR spectra of these isomers are essentially identical, only the lowest energy isomer is presented. Table 2 summarises the characteristics of the complexes including relative energies, dissociation energies (D_0), $Mn^+\cdots C$ bond lengths, and $\nu_1(a_1)$ vibrational frequencies.

3.2.1. $MnCH_4^+$

The different isomers for $MnCH_4^+$ are shown in Fig. 3. The 7-C(1) complex, which has an η^3 bonding configuration and C_{3v} symmetry, is predicted to lie lowest in energy, with the 5-C(1) complex, which has a similar η^3-bound C_{3v} structure, lying 56 kJ/mol higher in energy. Michelini et al. [17] found a smaller energy difference between the 7-C(1) and 5-C(1) complexes at the B3LYP/TZVP level (+42 kJ/mol), but a much larger difference at the CCSD(T)/TZVP level (+79 kJ/mol). The η^2 configuration for ^7S $Mn^+–CH_4$ is found to be a transition state lying 3 kJ/mol above the η^3 minimum. Calculations for other $TM^+–CH_4$ complexes demonstrate that an η^3 configuration is also adopted for Sc^+, Ti^+, V^+, Cr^+, Fe^+ and Zn^+ [8,10,26–30], whereas the η^2 configuration is preferred for Co^+, Ni^+ and Cu^+ [3,7,9–11,31].

For the 7-C(1) complex, the DFT calculations predict an intermolecular $Mn^+\cdots C$ bond length of 2.64 Å. The intermolecular bond is reasonably long because the Mn^+ 4s orbital is singly occupied and repulsive with respect to the filled $3a_1$ C–H bonding molecular orbital (MO) of CH_4 (one of the t_2 C–H bonding MOs in the free CH_4). This on-axis repulsion is alleviated somewhat in the 7-C(1) complex by partial $4s/4p_z$ hybridization (despite the high energy of the 4p orbitals), which transfers the 4s electron density away from the intermolecular region to the opposite side of the Mn^+ ion. Weis et al. [32] have previously documented this mechanism for the $Mn^+–H_2$ complex. The NPA analysis for the 7-C(1) cluster demonstrates that electron donation from the C–H bonding MOs of CH_4 to the Mn^+ ion is minimal; 0.02*e* is transferred from the $3a_1$ MO of CH_4 into the Mn^+ 4s, $3d_{z^2}$ and $4p_z$ orbitals, and 0.01*e* from the 1*e* MOs of CH_4 into the Mn^+ $3d_{yz}$ and $3d_{xz}$ orbitals. Therefore, the intermolecular cohesion in the 7-C(1) $Mn^+–CH_4$ complex is primarily due to electrostatic and induction interactions.

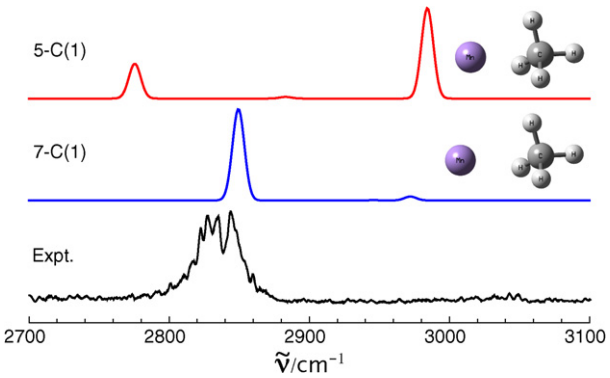

Fig. 4. Experimental IR photodissociation spectrum of $Mn^+–CH_4$ (lower) and the calculated spectra of the 7-C(1) (middle) and 5-C(1) (top) complexes. Intensities in the predicted spectrum for the 5-C(1) complex have been multiplied by a factor of 2.

For the 5-C(1) complex, the DFT calculations predict an intermolecular $Mn^+\cdots C$ bond length of 2.24 Å. This intermolecular bond is much shorter than in the 7-C(1) complex due to partial $4s/3d_{z^2}$ hybridization with concomitant transfer of 4s electron density into the *x*–*y* plane. As the 3d orbitals lie below the 4p orbitals, this hybridization scheme is more effective than $4s/4p_z$ hybridization at transferring the repulsive 4s electron density away from the bonding axis. Closer approach of the CH_4 ligand to the Mn^+ ion in the 5-C(1) complex leads, in turn, to greater electron donation from the CH_4 ligand to the metal ion (0.06*e*).

The inserted 7-I(1) and 5-I(1) isomers are both predicted to lie significantly higher in energy than the 7-C(1) complex (+163 and +102 kJ/mol, respectively). The 7-I(1) complex is less stable than the 5-I(1) complex in which the Mn^+ ion utilises the two $4s/3d_{x^2-y^2}$ hybrid orbitals to form covalent-like bonds with the H atom and CH_3 group.

We turn now to a comparison of the experimental IR-PD spectrum for $MnCH_4^+$ and the calculated spectra of the 7-C(1) and 5-C(1) complexes as shown in Fig. 4. Attaching a CH_4 molecule to the Mn^+ ion in an η^3 configuration reduces the symmetry from T_d to C_{3v} and transforms the methane molecule's vibrational modes. Most importantly, the $\nu_1(a_1)$ mode in $Mn^+–CH_4$ becomes slightly more localised on the three C–H bonds adjacent the ion and becomes IR active. The $\nu_3(t_2)$ mode is transformed into two infrared active modes designated $\nu_3(a_1)$ and $\nu_3(e)$. For the $\nu_3(a_1)$ mode the vibrational motion is mainly localised on the C–H bond pointing away from the ion, and is out of phase with respect to the motion of the other three C–H bonds. The doubly degenerate $\nu_3(e)$ mode primarily involves an antisymmetric stretching motion of the three C–H bonds pointing towards the ion.

The spectrum of the 7-C(1) complex is predicted to be dominated by a single peak at 2849 cm^{-1} (I = 90 km/mol), corresponding to the $\nu_1(a_1)$ vibration. The red-shift of this band from that of the free CH_4 molecule reflects a weakening and lengthening (by 0.007 Å) of the C–H bonds pointing towards the Mn^+ ion. The $\nu_3(e)$ and $\nu_3(a_1)$ vibrational modes are predicted to be associated with very weak transitions at 2945 cm^{-1} (I = 0.24 km/mol) and 2972 cm^{-1} (I = 4 km/mol), respectively.

The spectrum of the 5-C(1) complex is also predicted to contain three peaks corresponding to the $\nu_1(a_1)$, $\nu_3(e)$ and $\nu_3(a_1)$ vibrations. The $\nu_1(a_1)$ band is predicted to appear at 2775 cm^{-1} (I = 17 km/mol), substantially lower in frequency than for the 7-C(1) complex, with the marked reduction linked to enhanced electron donation from the CH_4 ligand, which is also signalled by a substantial 0.015 Å lengthening of the three C–H bonds pointing towards the Mn^+ ion.

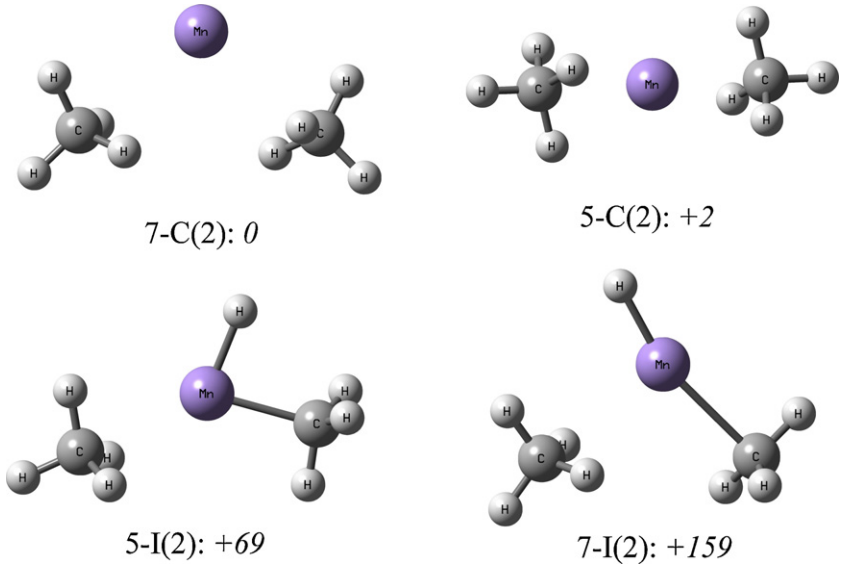

Fig. 5. DFT calculated isomers for $Mn(CH_4)_2^+$. Relative energies for each structure are given in kJ/mol.

For the 5-C(1) complex, the $\nu_3(a_1)$ band occurs at 2984 cm^{-1}, only slightly higher in frequency than for the 7-C(1) complex, but with a substantially larger IR intensity (I = 44 km/mol). The $\nu_3(e)$ band is expected to be very weak (I = 0.80 km/mol) and should occur at 2883 cm^{-1}.

Comparison of the experimental spectrum with predicted spectra for 7-C(1) and 5-C(1) (Fig. 4) demonstrates that only the former isomer is present in the experiment because the only feature in the $MnCH_4^+$ IR-PD spectrum is a single band centred at 2836 cm^{-1} corresponding closely with the predicted $\nu_1(a_1)$ band for the 7-C(1) complex. The $\nu_3(a_1)$ and $\nu_3(e)$ bands for the 7-C(1) complex are predicted to be respectively around 25 and 380 times weaker than the $\nu_1(a_1)$ band and are both indistinguishable from the background noise. There is no evidence for bands associated with the 5-C(1) complex in the IR-PD spectrum. This is not surprising as the 7-C(1) complex is predicted to be significantly lower in energy, with the 5-C(1) complex lying above the ^7S $Mn^+ + CH_4$ asymptote. In addition, absorption of a single IR photon by the 5-C(1) complex does not provide sufficient energy to access the ^5S $Mn^+ + CH_4$ asymptote.

The observed $\nu_1(a_1)$ band of $Mn^+–CH_4$, which has an overall width of ~30 cm^{-1}, displays hints of rotational sub-structure. Excitation of the $\nu_1(a_1)$ vibration corresponds to a parallel transition ($\Delta K = 0$ and $\Delta J = \pm 1$), suggesting that the structure is due to overlapping P and R branch ro-vibrational lines from several K sub-bands.

The observation that dissociation of $Mn^+–CH_4$ occurs following single-photon excitation of the $\nu_1(a_1)$ band allows one to set an upper limit of 2836 cm^{-1} (33.9 kJ/mol) on the binding energy of the 7-C(1) complex. A lower estimate for the binding energy can be obtained by noting that the $\nu_1(a_1)$ band-shift for $Mn^+–CH_4$ (-81 cm^{-1}) is larger in magnitude than that of $Al^+–CH_4$ (-67 cm^{-1}). If the binding energy is correlated with the vibrational band-shift, as it is for the $Mn^+–H_2$ and $Al^+–H_2$ complexes [33,34], one can deduce that the binding energy of $Mn^+–CH_4$ exceeds that of $Al^+–CH_4$ (25.3 kJ/mol [35]). The binding energy range deduced from experiment (25.3 kJ/mol $\leq D_0 \leq$ 33.9 kJ/mol) is compatible with theoretical estimates; on the basis of our DFT calculations the CH_4 binding energy of the 7-C(1) complex is found to be 34 kJ/mol, which is reduced to 30 kJ/mol when basis set superposition error is taken into account. Michelini et al. [17] calculated similar binding energies for the 7-C(1) complex: 33 and 34 kJ/mol at the B3LYP/TZVP and CCSD(T)/TZVP levels, respectively. In comparison, 5-C(1) has a predicted binding energy of 66 kJ/mol.

The $TM^+\cdots CH_4$ binding energy for ^7S Mn^+ is lower than those measured for Ti^+ (70 kJ/mol [8]), Fe^+ (73 kJ/mol [10]; 57 kJ/mol [36]), Co^+ (97 kJ/mol [9]; 90 kJ/mol [36]), and Ni^+ (104 kJ/mol [10]). This is a consequence of the repulsive half-filled 4s orbital of the Mn^+ cation. Despite Ti^+ and Fe^+ also having ground electronic states containing a 4s electron, promotion of this electron into a 3d orbital is substantially more favourable than for Mn^+ and occurs upon addition of the first CH_4 ligand [8,10].

3.2.2. $Mn(CH_4)_2^+$

Four different forms of the $Mn(CH_4)_2^+$ species were investigated through DFT calculations as shown in Fig. 5. In contrast to $Mn^+–CH_4$, for $Mn(CH_4)_2^+$ the two ion-molecule complexes of different spin multiplicity lie close in energy; the 7-C(2) complex is the global minimum with the 5-C(2) complex calculated to lie only 2 kJ/mol higher in energy. However, it is important to remember that the calculations underestimate the experimental ^7S–^5S separation for the bare Mn^+ ion. Both the 7-C(2) and 5-C(2) isomers have the two CH_4 ligands attached in η^3 configurations, but, as explained below, with different coordination geometries. The inserted 7-I(2) and 5-I(2) isomers were found to lie significantly higher in energy (>+69 kJ/mol), suggesting that the recorded IR-PD spectrum is associated with either 7-C(2) or 5-C(2) complexes.

For the 7-C(2) complex, the two ligands are attached such that the $C\cdots Mn^+\cdots C$ angle is 101° and have $Mn^+\cdots C$ bond lengths of 2.77 Å, slightly greater than for the 7-C(1) complex. The CH_4 ligands are arranged in such a way that the complex has C_2 symmetry. The near right-angle coordination of the ligands in 7-C(2) is favoured by their interaction with the $4p_z$ and $4p_x$ orbitals, which partially hybridize with the 4s orbital to shift its repulsive electron density away from the methane ligands. A similar mechanism was used to explain the bent structure of $Mn^+–(H_2)_2$ calculated by Weis et al. [32]. The calculated dissociation energy for the loss of a CH_4 ligand from 7-C(2) is 21 kJ/mol, around half the energy required to remove the second CH_4 to give the bare Mn^+ ion. Ligand–ligand repulsion in 7-C(2) may contribute to this substantial reduction.

In contrast to the bent structure of the 7-C(2) complex, the two CH_4 ligands in the 5-C(2) complex have a linear coordination. The ligands attach to opposite sides of the ion in an arrangement having D_{3d} symmetry and with $Mn^+\cdots C$ bond lengths of 2.11 Å. As described for 5-C(1), $4s/3d_{z^2}$ hybridization serves to transfer the repulsive 4s electron density away from the CH_4 ligands result-

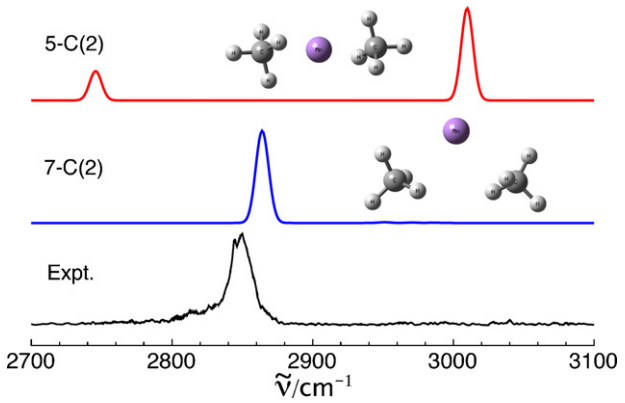

Fig. 6. Experimental IR photodissociation spectrum of Mn^+–$(CH_4)_2$ (lower) and the calculated spectra of the 7-C(2) (middle) and 5-C(2) (top) complexes. Intensities in the predicted spectrum for the 5-C(2) complex have been multiplied by a factor of 2.3.

ing in shorter intermolecular bond lengths for 5-C(2) compared to 7-C(2). The concerted polarization of the ^{5}S Mn^+ ion by the two linearly disposed methane ligands results in 5-C(2) being energetically competitive with 7-C(2) despite the excited electronic state of the core. The energy required to remove a CH_4 ligand from the 5-C(2) complex is predicted to be 74 kJ/mol, slightly more energy than required to remove the next CH_4. An increased binding energy for the second ligand compared to the first has been observed for other TM^+–$(CH_4)_2$ and TM^+–$(H_2)_2$ complexes where the penalty for $4s/3d_{z^2}$ hybridization can be shared between two ligands [7,37].

The experimental IR-PD spectrum for $Mn(CH_4)_2^+$ and the calculated IR spectra of 7-C(2) and 5-C(2) are compared in Fig. 6. The characteristics of the IR spectra for the 7-C(2) and 5-C(2) complexes are very similar to those described for the 7-C(1) and 5-C(1) complexes, respectively. Only one main band is present for 7-C(2), centred at 2864 cm^{-1}, corresponding to $\nu_1(a_1)$ vibrations. On the other hand, two prominent bands are predicted for 5-C(2), one at 2746 cm^{-1} due to a $\nu_1(a_1)$ vibration, and the other at 3010 cm^{-1} due to a $\nu_3(a_1)$ vibration. The IR-PD spectrum of $Mn(CH_4)_2^+$ displays just a single dominant band at 2849 cm^{-1}, which is clearly only compatible with the predicted spectrum for the 7-C(2) complex.

Although the 5-C(2) complex is predicted to be essentially isoenergetic with the 7-C(2) complex, there is no evidence for it contributing to the experimental IR-PD spectrum. Although this may seem to exclude its presence in our experiment, other factors may be at play. For example, dissociation of 5-C(2) while conserving spin multiplicity to the 5-C(1)+ CH_4 asymptote requires 74 kJ/mol (~6200 cm^{-1}) of energy, considerably more energy than is provided by a single IR photon in the 3 μm region. Consequently, transitions for the 5-C(2) complex are unlikely to appear in the single-photon IR-PD spectrum. On the other hand, if the vibrationally excited quintet PES was coupled with the septet PES, the photo-excited 5-C(2) complex would posses sufficient energy to dissociate to the 7-C(1)+ CH_4 asymptote and would be detected. Despite rapid crossing between PESs of different spin multiplicity being observed for several $TM^+\cdots(CH_4)_n$ complexes [13,8], the absence of spin–orbit coupling mechanisms for the 5-C(2) and 7-C(2) complexes may inhibit this process.

3.2.3. $Mn(CH_4)_3^+$

The four isomers investigated for the $Mn(CH_4)_3^+$ species are shown in Fig. 7. In line with the results for the $n = 1$ and 2 species, the 7-C(3) complex is predicted to be the global minimum with the 5-C(3) complex lying 12 kJ/mol higher in energy. The 7-I(3) and 5-I(3) isomers are predicted to lie considerably higher in energy (≥59 kJ/mol), probably excluding their presence in our experiment.

The 7-C(3) complex, which possesses C_3 symmetry, has all three CH_4 molecules attached in an η^3 configuration, with the three $Mn^+\cdots C$ bonds being approximately at right angles to one other (99°). The 7-C(3) complex exhibits a similar bonding pattern to the 7-C(1) and 7-C(2) complexes; the CH_4 ligands concertedly polarise the repulsive 4s electron density away from the intermolecular

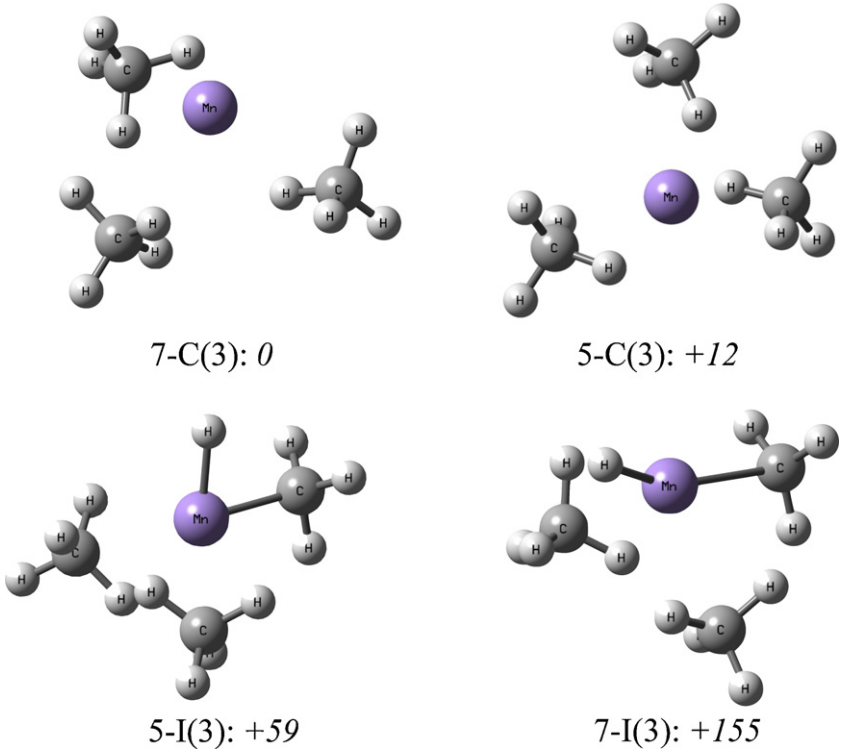

Fig. 7. DFT calculated isomers for $Mn(CH_4)_3^+$. The relative energies for each structure are also given in kJ/mol.

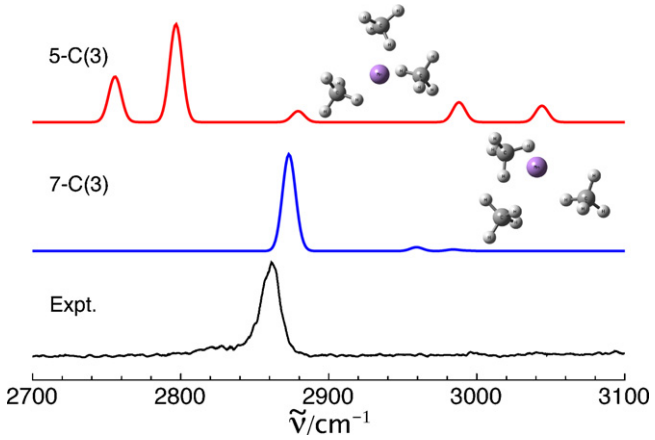

Fig. 8. Experimental IR photodissociation spectrum of Mn^+–$(CH_4)_3$ (lower) and the calculated spectra of the 7-C(3) (middle) and 5-C(3) (top) complexes. Intensities in the predicted spectrum for the 5-C(3) complex have been multiplied by a factor of 4.4.

region through partial 4s/4p hybridization. This geometry and bonding pattern parallels that evoked for Mn^+–$(H_2)_3$ by Weis et al. [32]. Compared to 7-C(2) there is an increase in the $Mn^+\cdots C$ bond lengths from 2.77 to 2.87 Å, coupled with a decrease in the CH_4 binding energy from 21 to 13 kJ/mol. Ligand–ligand repulsion may be responsible for the significant step-wise decrease binding energy from 7-C(1) to 7-C(3).

The 5-C(3) complex is distinguished by having CH_4 ligands bound in an η^2 rather than an η^3 configuration. Overall, the complex has C_{2v} symmetry. The CH_4 ligands are attached in a near T-shaped coordination, with two equivalent ligands bound to the ion approximately opposite to one another ($C\cdots Mn^+\cdots C$ angle of 153°) and $Mn^+\cdots C$ bond lengths of 2.30 Å. The third ligand is attached between the equivalent ligands, disrupting the linear arrangement found for $n=2$. The $Mn^+\cdots C$ bond is much longer for this third ligand (2.61 Å) which can be rationalised by noting that this ligand is situated in a region in which it interacts repulsively with the $4s/3d_{z^2}$ hybrid orbital induced by the first two ligands. Consequently, there is a profound drop in the CH_4 binding energy in 5-C(3) (3 kJ/mol) compared to 5-C(2) (74 kJ/mol). A similar drop in binding energy from $n=2$ to 3 has been observed for the Fe^+–$(CH_4)_n$ complexes [10], with an IR-PD study confirming that the $n=3$ structure has a similar T-shaped geometry as proposed here for 5-C(3) [16].

The experimental IR-PD spectrum of $Mn(CH_4)_3^+$ and the predicted IR spectra for the 7-C(3) and 5-C(3) complexes are shown in Fig. 8. Obviously, the IR-PD spectrum, which displays a single band at 2861 cm^{-1}, matches the predicted spectrum for the 7-C(3) complex. There are no signs of absorption features in the 2720–2820 cm^{-1} region, excluding the presence of the 5-C(3) complex, which would give rise to bands in this range. Note that for the 5-C(3) complex, dissociation along a spin-allowed pathway would be energetically possible following single-photon IR excitation.

3.2.4. $Mn(CH_4)_n^+$ ($n=4$–6)

As outlined above, the $Mn(CH_4)_n^+$ ($n=1$–3) IR-PD spectra clearly correspond to the predicted spectra for the 7-C(n) complexes leading one to suspect that the larger clusters probably also possess a ^{7}S Mn^+ core. Indeed, as seen in Fig. 9, spectra of the $Mn(CH_4)_n^+$ ($n=4$–6) complexes in the C–H stretch region are also dominated by a single band and are therefore also most probably associated with 7-C(n) complexes. The predicted lowest energy forms of the 7-C(4), 7-C(5) and 7-C(6) complexes are shown in Fig. 10 where it can be seen that in each case the methane ligands are attached in a η^3 configuration to the central Mn^+ ion.

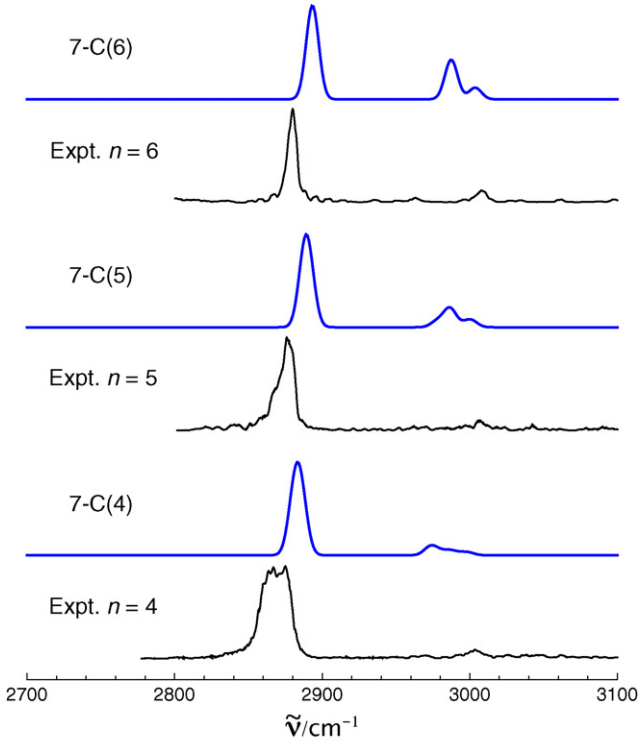

Fig. 9. Experimental IR photodissociation spectra of Mn^+–$(CH_4)_n$ ($n=4$–6) (black) and calculated spectra of the 7-C(n) (blue) complexes. (For interpretation of the references to color in this figure legend, the reader is referred to the web version of the article.)

The $\nu_1(a_1)$ vibrational bands of the $n=4$–6 complexes occur at 2870, 2876 and 2880 cm^{-1} in excellent agreement with predicted bands for the 7-C(4), 7-C(5) and 7-C(6) clusters at 2883, 2889 and 2893 cm^{-1} (Fig. 9). As well, weaker peaks, assignable to the $\nu_3(a_1)/(e)$ vibrations, are observed at 3003, 3006 and 3008 cm^{-1}. There is no evidence for peaks that would correspond to complexes containing a ^{5}S Mn^+ core.

The 7-C(4) complex is predicted to have C_2 symmetry, with two equivalent η^3-bound CH_4 molecules sitting approximately opposite to one another such that the $C\cdots Mn^+\cdots C$ angle is 151°; these two ligands can be thought of as being attached to opposite lobes of the $4p_z$ orbital. The other two CH_4 ligands can be viewed as being attached to single lobes of $4p_x$ and $4p_y$ orbitals and are disposed such that the angle between their $Mn^+\cdots C$ bonds are 98° with respect to one another. The $Mn^+\cdots C$ intermolecular bonds for the ligands attached opposite to one another are slightly longer than the intermolecular bonds for the other two ligands (3.09 c.f. 2.95 Å). The bond length difference can be rationalised by realising that the 4p orbitals hybridize with the 4s orbital to transfer electron density away from the intermolecular region to allow closer approach of the CH_4 ligands. This hybridization will obviously be ineffective at reducing the 4s electron density in the intermolecular region for the two CH_4 ligands attached to opposite lobes of the $4p_z$ orbital. The CH_4 binding energy of 7-C(4) is predicted to be 8 kJ/mol.

For the 7-C(5) cluster, the methane ligands are attached in a trigonal bipyramidal coordination geometry (C_{3h} symmetry). The axial and equatorial ligands, both bound in an η^3 configuration, have $Mn^+\cdots C$ bond lengths of 3.16 and 3.10 Å, respectively. The CH_4 binding energy of 7-C(5) is calculated to be 5 kJ/mol. This spherical geometry is most likely adopted by 7-C(5) because the need to minimise ligand–ligand repulsion outweighs the benefit of $4s/4p_z$ hybridization to reduce 4s-ligand repulsion. A trigonal bipyramid coordination geometry was not predicted for the Al^+–$(CH_4)_5$ clus-

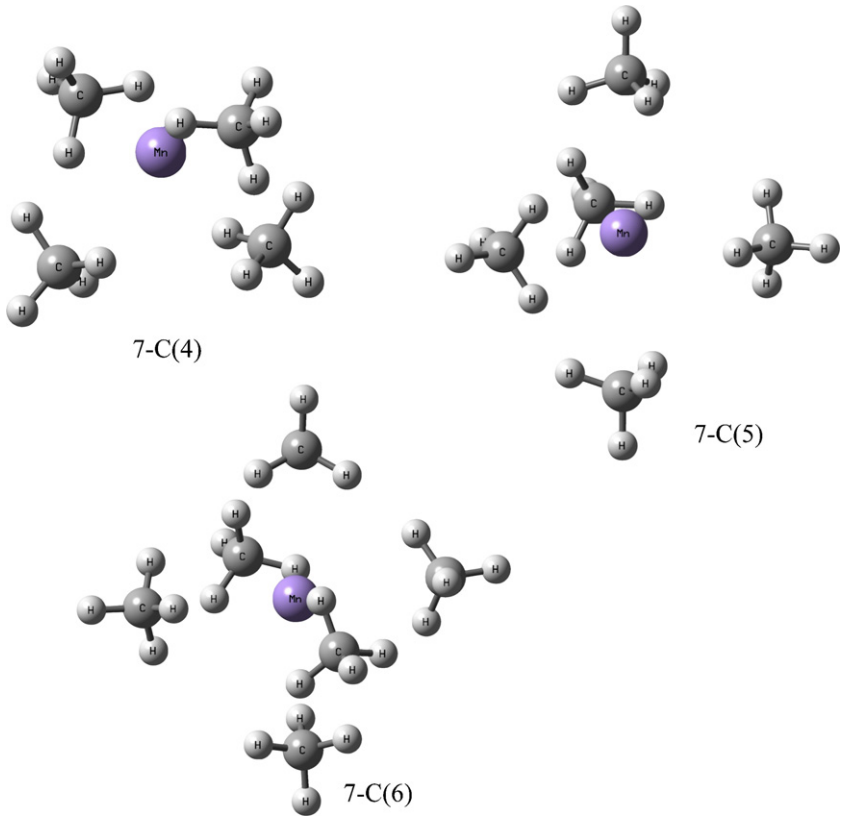

Fig. 10. DFT calculated isomers for $Mn(CH_4)_n^+$ (n = 4–6).

ter, which has the methanes attached at ~90° to one another [15]. For Al^+–$(CH_4)_5$ the preference for partial 3s/3p hybridization to polarise the 3s electron density so that it occupies a region away from the ligands may be connected to the fact that the 3s–3p energy difference in Al^+ is slightly smaller than the 4s–4p difference in Mn^+ [24]. However, it is also possible that the trigonal bipyramidal geometry of 7-C(5) is an artefact of the DFT method, which fails to account for dispersion forces between the CH_4 ligands and therefore emphasizes ligand–ligand repulsion compared to the MP2 method employed for Al^+–$(CH_4)_5$.

For 7-C(6) the η^3 CH_4 ligands attach to Mn^+ in an octahedral coordination geometry with D_3 symmetry. The attached ligands have $Mn^+\cdots C$ bond lengths of 3.21 Å, with the complex having a CH_4 binding energy of 4 kJ/mol. A similar octahedral coordination geometry was also deduced for Al^+–$(CH_4)_6$ [15].

4. Conclusions

In summary, the IR-PD spectra for the $Mn(CH_4)_n^+$ (n = 1–6) complexes feature a single main band, appearing at 2836 cm^{-1} for n = 1 and progressively shifting to higher frequency as n increases. DFT calculations performed for various structural isomers of the $Mn(CH_4)_n^+$ species demonstrate that the clusters contain CH_4 ligands bound in an η^3 configuration to the Mn^+ ion in its ground ^7S electronic state. In general, the ligands attach at approximate right angles to one another, eventually establishing an octahedral coordination for n = 6, although the n = 5 complex was found to adopt a trigonal bipyramidal coordination geometry, rather than following this bonding pattern. The positioning of the ligands on the same side of the Mn^+ ion for n = 2–4 is due to their repulsive interaction with the half-filled Mn^+ 4s orbital and the subsequent partial 4s/4p hybridization which displaces 4s electron density away from the ligands.

The predicted IR spectra for the ^7S Mn^+ ion-molecule complexes match the measured IR-PD spectra, with, in each case, the main band being assigned to the totally symmetric $\nu_1(a_1)$ C–H stretching vibrations of the attached methane molecules. The n = 1–3 IR-PD spectra display no evidence for ion-molecule complexes containing the Mn^+ in its ^5S electronic state, even though for n = 2 this isomer is predicted to lie only slightly higher in energy than the complex containing Mn^+ in its ^7S state.

Acknowledgments

The authors are grateful to the Australian Research Council and University of Melbourne for supporting this research. Computing resources provided by the Victorian Partnership for Advanced Computing and the NCI National Facility in Canberra are gratefully acknowledged.

References

[1] A.E. Shilov, G.B. Shul'pin, Chemical Reviews 97 (1997) 2879–2932.
[2] J. Roithova, D. Schröder, Chemical Reviews 110 (2) (2009) 1170–1211.
[3] J.K. Perry, G. Ohanessian, W.A. Goddard III, Journal of Physical Chemistry 97 (1993) 5238–5245.
[4] H. Wu, W. Zhou, T. Yildirim, Journal of the American Chemical Society 131 (2009) 4995–5000.
[5] P.D.C. Dietzel, V. Besikiotis, R. Blom, Journal of Materials Chemistry 19 (2009) 7362–7370.
[6] R.H. Schultz, P.B. Armentrout, Journal of Physical Chemistry 97 (1993) 596–603.
[7] C.L. Haynes, P.B. Armentrout, J.K. Perry, W.A. Goddard III, Journal of Physical Chemistry 99 (1995) 6340–6346.
[8] P.A.M. van Koppen, J.K. Perry, P.R. Kemper, J.E. Bushnell, M.T. Bowers, International Journal of Mass Spectrometry 187 (1999) 989–1001.
[9] Q. Zhang, P.R. Kemper, S.K. Shin, M.T. Bowers, International Journal of Mass Spectrometry 204 (2001) 281–294.
[10] Q. Zhang, P.R. Kemper, M.T. Bowers, International Journal of Mass Spectrometry 210–211 (2001) 265–281.
[11] F. Liu, X.G. Zhang, P.B. Armentrout, Physical Chemistry Chemical Physics 7 (2005) 1054–1064.

[12] K.K. Irikura, J.L. Beauchamp, Journal of Physical Chemistry 95 (21) (1991) 8344–8351.
[13] H. Schwarz, International Journal of Mass Spectrometry 237 (2004) 75–105.
[14] N.R. Walker, R.S. Walters, M.A. Duncan, New Journal of Chemistry 29 (2005) 1495–1503.
[15] B.L.J. Poad, C.D. Thompson, E.J. Bieske, Chemical Physics 346 (2008) 176–181.
[16] R.B. Metz, Advances in Chemical Physics 138 (2008) 331–373.
[17] M.D. Michelini, N. Russo, E. Sicilia, Journal of Physical Chemistry A 106 (2002) 8937–8944.
[18] M.D. Michelini, E. Sicilia, N. Russo, M.E. Alikhani, B. Silvi, Journal of Physical Chemistry A 107 (2003) 4862–4868.
[19] C.D. Thompson, C. Emmeluth, B.L.J. Poad, G.H. Weddle, E.J. Bieske, Journal of Chemical Physics 125 (2006), 044310-5.
[20] M.J. Frisch, et al., Gaussian 09, Revision A.1, 2009.
[21] M. Dolg, U. Wedig, H. Stoll, H. Preuss, Journal of Chemical Physics 86 (1987) 866–872.
[22] J.M.L. Martin, A. Sundermann, Journal of Chemical Physics 114 (2001) 3408–3420.
[23] E.D. Glendening, A.E. Reed, J.E. Carpenter, F. Weinhold, NBO version 3.1, 1985.
[24] Y. Ralchenko, A. Kramida, J. Reader, N.A. Team, (2008) NIST Atomic Spectra Database (version 3.1.5), [Online]. Available: http://physics.nist.gov/asd3. National Institute of Standards and Technology, Gaithersburg, MD.
[25] R.A. Toth, L.R. Brown, R.H. Hunt, L.S. Rothman, Applied Optics 20 (1981) 932–935.
[26] N. Russo, E. Sicilia, Journal of the American Chemical Society 123 (2001) 2588–2596.
[27] E. Sicilia, N. Russo, Journal of the American Chemical Society 124 (2002) 1471–1480.
[28] M. Hendrickx, K. Gong, L. Vanquickenborne, Journal of Chemical Physics 107 (1997) 6299–6305.
[29] S. Chiodo, O. Kondakova, M.D. Michelini, N. Russo, E. Sicilia, A. Irigoras, J.M. Ugalde, Journal of Physical Chemistry A 108 (2004) 1069–1081.
[30] W.Y. Lu, T.H. Wong, P.D. Kleiber, Chemical Physics Letters 347 (2001) 183–188.
[31] P. Mâitre, C.W. Bauschlicher, Journal of Physical Chemistry 97 (1993) 11912–11920.
[32] P. Weis, P.R. Kemper, M.T. Bowers, Journal of Physical Chemistry A 101 (1997) 2809–2816.
[33] V. Dryza, B.L.J. Poad, E. Bieske, Journal of Physical Chemistry A 113 (2009) 6044–6048.
[34] C. Emmeluth, B.L.J. Poad, C.D. Thompson, G.H. Weddle, E.J. Bieske, A.A. Buchachenko, T.A. Grinev, J. Kłos, Journal of Chemical Physics 127 (2007) 164310.
[35] P.R. Kemper, J. Bushnell, M.T. Bowers, G.I. Gellene, Journal of Physical Chemistry 102 (1998) 8590–8597.
[36] P. Armentrout, B. Kickel, in: B. Freiser (Ed.), Organometallic Ion Chemistry, Kluwer Academic, Dordrecht, The Netherlands, 1996.
[37] P.R. Kemper, P. Weis, M.T. Bowers, P. Mâitre, Journal of the American Chemical Society 120 (1998) 13494–13502.